Biomedicine & Pharmacotherapy 175 (2024) 116626

Contents lists available at ScienceDirect

Biomedicine & Pharmacotherapy

journal homepage: www.elsevier.com/locate/biopha

Designing multitarget ligands for neurodegenerative diseases with improved permeability trough PLGA nanoencapsulation

Vanesa Nozal [a,1,2], Paula Fernández-Gómez [b,2], Alfonso García-Rubia [a], Loreto Martínez-González [a,c], Eva P. Cuevas [a,c], Eva Carro [c,d], Valle Palomo [b,c,e,*], Ana Martínez [a,c,**]

[a] Centro de Investigaciones Biológicas Margarita Salas-CSIC, Ramiro de Maeztu 9, Madrid 28040, Spain
[b] Instituto Madrileño de Estudios Avanzados en Nanociencia (IMDEA Nanociencia), Madrid 28049, Spain
[c] Centro de Investigación Biomédica en Red de Enfermedades Neurodegenerativas (CIBERNED), Instituto de Salud Carlos III, Madrid 28031, Spain
[d] Neurobiology of Alzheimer's Disease Unit, Functional Unit for Research into Chronic Diseases, Instituto de Salud Carlos III, Madrid 28029, Spain
[e] Unidad de Nanobiotecnología Asociada al Centro Nacional de Biotecnología (CSIC), Madrid 28049, Spain

ARTICLE INFO

Key words:
Multitarget ligand
Blood-brain barrier
Nanoparticles
Protein kinase inhibitors
Alzheimer's disease
Amyotrophic lateral sclerosis

ABSTRACT

Multitarget ligands (MTLs) have emerged as an interesting alternative for addressing complex multifactorial pathologies such as neurodegenerative diseases. However, a common challenge associated with these compounds is often their high molecular weight and low solubility, which becomes a hurdle when trying to permeate over the blood-brain barrier (BBB). In this study, we have designed two new MTLs that modulate three pharmacological targets simultaneously (tau, beta-amyloid and TAR DNA-binding protein 43). To enhance their brain penetration, we have formulated organic polymeric nanoparticles using poly(lactic-co-glycolic acid). The characterization of the formulations, evaluation of their permeability through an *in vitro* BBB model, and assessment of their activity on disease-representative cellular models, such as Alzheimer's disease and amyotrophic lateral sclerosis, have been conducted. The results demonstrate the potential of the new MTLs and their nanoparticle encapsulation for the treatment of neurodegenerative diseases.

1. Introduction

Multitarget ligands (MTLs) are chemical entities bearing different pharmacophores that enable the simultaneous binding to more than one protein or biological target. These compounds have been proposed as an interesting approach for the treatment of complex conditions such as neurodegenerative diseases (NDs) [1,2], bacterial infections or cancer [3].

NDs cause the progressive loss of specific neuronal populations in the central nervous system (CNS), leading to different symptoms in the patients. This gradual neuronal death is believed to be triggered by multiple factors including protein aggregation, inflammation, oxidative stress or excitotoxicity. Protein aggregation seems to be disease-specific, and is classified according to the predominant protein found in the aggregates. Alzheimer's disease (AD) presents two main pathological hallmarks: neurofibrillary tangles, composed of hyperphosphorylated protein tau and senile plaques formed by amyloid beta fibrils [4]. In amyotrophic lateral sclerosis (ALS), motor neurons display cytoplasmic deposits of hyperphosphorylated TAR DNA-binding protein of 43 KD (TDP-43), accompanied by a reduction in nuclear levels of this protein [5]. TDP-43 has recently emerged as a central target in neurodegeneration, as it has been found aggregated in other pathologies, including AD, [6] leading to the classification of a new form of dementia called limbic-predominant age-related TDP-43 encephalopathy (LATE). LATE is often misdiagnosed as AD due to the similarity in symptoms experienced by patients [7]. Given the central role of these hallmarks in the course of the diseases, modulators of these three pathological cascades (beta-amyloid, tau and TDP-43) might represent an innovative and effective treatment for these fatal conditions.

While the cause of aggregate formation remains unknown, their

* Corresponding author at: Instituto Madrileño de Estudios Avanzados en Nanociencia (IMDEA Nanociencia), Madrid 28049, Spain.
** Corresponding author at: Centro de Investigaciones Biológicas Margarita Salas-CSIC, Ramiro de Maeztu 9, Madrid 28040, Spain.
E-mail addresses: valle.palomo@imdea.org (V. Palomo), ana.martinez@csic.es (A. Martínez).
[1] Current address: Laboratory of Medicinal Chemistry, Department of Pharmaceutical Sciences, University of Antwerp, Universiteitsplein 1, 2610, Antwerp, Belgium
[2] These authors share first authorship.

https://doi.org/10.1016/j.biopha.2024.116626
Received 5 January 2024; Received in revised form 3 April 2024; Accepted 17 April 2024
Available online 24 April 2024

hyperphosphorylation together with the aberrant expression of some protein kinases has led to kinase inhibitors being identified as promising drug candidates against these diseases [8,9]. Consequently, numerous small molecules with this mode of action have been developed for the treatment of these NDs [8,10]. Notably, glycogen synthase kinase 3 (GSK-3) inhibitors advanced to clinical trials for AD due to their capacity to reduce tau phosphorylation in preclinical models [11,12]. Results from clinical phase II studies showed the target engagement of tideglusib, a selective GSK-3 inhibitor, demonstrating a reduction of phospho-tau in cerebrospinal fluid of AD patients [13]. Furthermore, inhibitors of casein kinase 1 (CK1) have not only shown to reduce pathological aggregates of phosphorylated TDP-43 but also to recover TDP-43 functional homeostasis in cells derived from patients [14] and to preserve motorneurons in the spinal cord of transgenic mice [15]. Lastly, leucine-rich repeated kinase 2 (LRRK2) inhibitors, beyond their clinical development for Parkinson's disease [16], have exhibited efficacy in reducing tau phosphorylation *in vivo* [17] and ameliorating disease burden in multiple sclerosis models [18].

However, given the multifactorial nature of these diseases, several pathological pathways are already widely activated by the time of diagnosis is made, being extremely complicated to restore several pathways by only targeting one of them. Our hypothesis is that multitarget drugs, which simultaneously modulate different targets, may produce a stronger pharmacological effect in patients. Specifically, the combination of different kinase inhibitors into a single molecule might represent an alternative approach, resulting in a new and improved therapy. Recently, our group has validated this strategy reporting the discovery of new MTLs, which presented the ability to inhibit key kinases involved in the development of pathological hallmarks of AD at the same time as interfere with the beta-amyloid pathology (Fig. 1) [19].

In this work, we aimed to extend the application of this approach to other NDs such as ALS. The primary focus of the new MTLs would be on key protein kinases involved in the phosphorylation of TDP-43. In addition to the previously mentioned CK1 and LRRK2, we also targeted tau and tubulin kinase 1 (TTBK1), one of the four kinases directly involved in the hyperphosphorylation of TDP-43 observed in ALS and frontotemporal dementia (FTD) patients [20]. In addition, recognizing that the main limitation of these interesting molecules lies in their poor central nervous system (CNS) permeability due to their high molecular weight and large polar surface areas, we proposed an encapsulation strategy involving the development of organic polymeric nanoparticles. We selected poly-lactic-co-glycolic acid (PLGA) nanoparticles (NPs) as more than 60 different compositions are currently available in the market for several conditions [21]. These NPs present excellent biocompatibility and controlled-release capabilities, thereby enhancing the drug's availability and efficacy at the target site of action.

2. Materials and methods

2.1. Chemistry

All the reagents were purchased from commercial sources and used without further purification. Purifications of crudes were performed with the indicated solvent as eluent by flash column chromatography carried out at medium pressure using either silica gel (E. Merck, grade 60, particle size 0.040−0.063 mm, 230−240 mesh ASTM) or the IsoleraOne flash purification system from Biotage. ^{1}H and ^{13}C nuclear magnetic resonance (NMR) data were obtained from a Bruker AV300 or AV500 MHz spectrometer. Chemical shifts, δ, expressed in parts per million (ppm) were calculated taking the reference of the appropriated deuterated solvents. Signal multiplicities (bs = broad signal, s = singlet, d = doublet, dd = doublet of doublets, ddd = doublet of doublet of doublets, t = triplet, td = triplet of doublets and m = multiplet) and coupling constants (J, Hz) are indicated for each molecule. Acquired spectroscopic data were analysed with MestreNova 11.0 software. The microwave-assisted synthesis was carried out using a Biotage Initiator eight single-mode cavity instrument from Biotage. Experiments were performed with the temperature control mode in sealed microwave process vials. The temperature was measured with an IR sensor on the outside of the reaction vessel. Stirring was provided by an *in situ* magnetic stirrer. High-performance liquid chromatography (HPLC) analyses were performed in a Thermo Finnigan Surveyor UV−vis Plus detector coupled with FinniganTM LXQ TM system. The column used for the analysis was a SunFire C18 (3.5 μm, 4.6 × 50 mm), and UV−vis spectra of the samples were acquired. Melting points were determined in a Büchi Melting Point M-560 device. High-resolution mass spectrometry (HRMS) was done in an Agilent 6500 spectrometer using positive electrospray techniques (ESI). Values are expressed in mass units (m/z). Elemental analyses were performed by the analytical department at CAI-UCM using the analyser LECO CHNS-932, and the results obtained were within ±0.4 % of the theoretical values. All the final compounds have purities ≥ 95 % as tested by HPLC.

Compounds **6** and **7** were synthesized according to the reported procedure by Nozal et al., 2021 [3].

2.1.1. N-(4-(prop-2-yN-1-yloxy)phenyl)-7 H-pyrrolo[2,3-d]pyrimidin-4-amine (5)

1 eq of 6-chloro-7-deazapurine, 1 eq of 4-propargylaniline and 0.1 eq of indium trichloride were dissolved in 2 mL of acetonitrile. The reaction was stirred under microwave irradiation at 100 ºC for 2 hours. The crude was dissolved in ethyl acetate (20 mL) and washed three times with water and saturated NaCl solution. The organic layers were dried over $MgSO_4$ and evaporated under high vacuum. The crude was purified using flash chromatography and CH_2Cl_2:MeOH 40:1 as eluents to afford a white solid (69 % yield). m.p. 217–218 ºC. ^{1}H-NMR (300 MHz, DMSO-d_6) δ (ppm): 11.70 (s, 1 H), 9.19 (s, 1 H), 8.21 (s, 1 H), 7.74 (dt, J = 9.5,

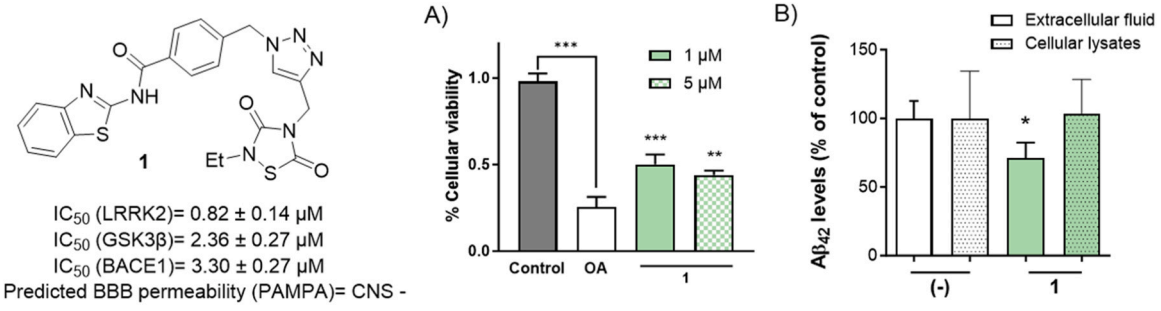

Fig. 1. Multitarget ligand **1** previously synthetized and validated in representative AD cellular models. Compound **1** has three different biological activities: inhibition of LRRK2, GSK-3 and beta-secretase 1 (BACE1), but poor brain permeability. A) Effect of compound **1** on the viability of SH-SY5Y cells treated with okadaic acid (OA) (in white) B) Reduction in the levels of beta-amyloid 42 ($A\beta_{42}$) in SK-APP cell line after 48 h treatment with MTL **1** at 10 μM. [19] Data are presented as the mean ± SEM of three independent experiments *(*** $p < 0.001$, ** $p < 0.01$, * $p < 0.05$).*

3.4 Hz, 2 H) 7.19 (dd, J = 3.5, 2.3 Hz, 1 H), 6.98 (dd, J = 9.0, 3.4 Hz, 2 H), 6.70 (dd, J = 3.5, 1.9 Hz, 1 H), 4.77 (d, J = 2.4 Hz, 2 H), 3.57 (t, J = 2.3 Hz, 1 H). ^{13}C-NMR (75 MHz, DMSO-d_6): δ (ppm) 153.7, 152.6, 150.8, 150.7, 134.0, 122.1, 121.8, 114.8, 103.2, 98.7, 79.5, 78.1, 55.6. Anal. Calcd. for $C_{15}H_{12}N_4O$: C, 68.17; H, 4.58; N, 21.20. Found: C, 67.86; H, 4.63; N, 21.23.

2.1.2. Synthesis of triazoles (8, 9)

1 eq of alkyne 1 and 1 eq of the corresponding azide (**6** or **7**) were dissolved in dimethyl formamide (DMF) in the presence of 10 % mol $CuSO_4{\cdot}5\ H_2O$, 10 % mol tris(benzyltriazolylmethyl)amine, and 20 % mol sodium ascorbate. The mixture was stirred overnight at room temperature. The crude was extracted using CH_2Cl_2:MeOH 9:1, washed with 5 % ammonium hydroxide solution and dried over $MgSO_4$. The crude was purified using flash chromatography on silica gel (CH_2Cl_2: MeOH 10:1).

2.1.2.1. 4-((4-((4-((7 H-pyrrolo[2,3-d]pyrimidin-4-yl)amine)phenoxy) methyl)-1 H-1,2,3-triazol-1-il)methyl)-N-(benzo[d]thiazol-2-yl)benzamide (8).. White solid, 28 % yield, m.p. 284–285 °C (dec.). ^{1}H-RMN (300 MHz, DMSO-d_6) δ (ppm): 12.91 (s, 1 H), 11.68 (s, 1 H), 9.17 (s, 1 H), 8.37 (s, 1 H), 8.21 (s, 1 H), 8.14 (d, J = 8.4 Hz, 2 H), 8.02 (dd, J = 8.0, 1.2 Hz, 1 H), 7.78 (d, J = 8.1 Hz, 1 H), 7.74 (dd, J = 9.0, 5.0 Hz, 2 H), 7.52–7.43 (m, 3 H), 7.34 (td, J = 7.6, 1.2 Hz, 1 H), 7.18 (dd, J = 3.5, 2.3 Hz, 1 H), 7.03 (d, J = 9.1 Hz, 2 H), 6.69 (dd, J = 3.5, 1.9 Hz, 1 H), 5.75 (s, 2 H), 5.15 (s, 2 H). ^{13}C-RMN (75 MHz, DMSO-d_6) δ (ppm): 153.7, 153.5, 150.9, 150.7, 143.3, 140.8, 133.7, 128.8, 128.0, 126.2, 124.9, 123.7, 122.2, 121.8, 114.7, 103.2, 98.8, 61.3, 52.4. ESI calcd for $C_{30}H_{24}N_9O_2S$ $[M + H]^+$ 574.1768 found 574.1760.

2.1.2.2. 2-(4-((4-((4-((7 H-pyrrolo[2,3-d]pyrimidin-4-yl)amine)phenoxy)methyl)-1 H-1,2,3-triazol-1-il)methyl)phenyl)-N-(benzo[d]thiazol-2-yl)acetamide (9). White solid, 22 % yield, m.p. 296–297 °C (dec.). ^{1}H-RMN (300 MHz, DMSO-d_6) δ (ppm): 12.59 (s, 1 H), 11.70 (s, 1 H), 9.20 (s, 1 H), 8.28 (s, 1 H), 8.20 (s, 1 H), 7.96 (dd, J = 8.4, 1.2 Hz, 1 H), 7.73 (t, J = 8.0 Hz, 3 H), 7.43 (td, J = 7.5, 1.5 Hz, 1 H), 7.39–7.26 (m, 5 H), 7.19 (dd, J = 3.5, 2.3 Hz, 1 H), 7.01 (d, J = 8.4 Hz, 2 H), 6.68 (dd, J = 3.5, 1.9 Hz, 1 H), 5.60 (s, 2 H), 5.11 (s, 2 H), 3.83 (s, 2 H). ^{13}C-RMN (75 MHz, DMSO-d_6) δ (ppm): 170.5, 158.3, 154.09, 154.06, 151.2, 151.06, 149.0, 143.7, 135.1, 131.9, 130.3, 128.6, 126.6, 125.0, 124.0, 122.2, 121.8, 114.7, 103.2, 98.8, 61.3, 52.4. ESI calcd for $C_{31}H_{26}N_9O_2S$ $[M + H]^+$ 588.1925 found 588.1930.

2.1.3. Organic nanoparticle formulation

Poly(lactic-co-glycolic acid) copolymer, ester terminated (nominal), Part.#B6010–4 P) with a 50:50 ratio (PLA/PGA), was purchased from Absorbable Polymers, Birmingham, USA. Polyvinyl alcohol (PVA, Mw 31,000–50,000, 87–89 % hydrolyzed, Cat. Number 363073) from Sigma Aldrich. Dimethyl sulfoxide (DMSO) and acetonitrile were purchased from other commercial sources.

2.1.3.1. Multitarget-loaded PLGA nanoparticles preparation by nanoprecipitation. 50 mg of PLGA copolymer were dissolved with magnetic stirring in 5 mL of acetone for 2 h at room temperature and mixed with 5–10 mg of the MTL in 5 mL of acetone:DMSO. The mixture was added dropwise (600 μL/min) over 20 mL of aqueous solution containing 2 % w/v PVA. The resulting emulsion was stirred for 2–3 h at room temperature. Finally, NPs were collected by centrifugation (Sorvall RC-5 C Centrifuge, SS-34 Rotor) at 15,000 rpm for 10 min and washed out three-to-four times with deionized water, frozen at −80 °C and lyophilized using a fast-freeze flask (Labconco Corp. 750 mL, Kansas, MO, USA) at −45 °C and $3.2{\cdot}10^{-2}$ mbar pressure.

2.1.4. Characterization of polymeric nanoparticles

2.1.4.1. Scanning electron microscopy (SEM). The morphology of the NPs was analyzed by SEM using a JEOL JSM 7600 F microscope (JEOL, Tokyo, Japan). For the analysis, lyophilized samples were fixed onto a sample holder and gold-coated for 90 s.

2.1.4.2. Dynamic light scattering (DLS). It was used to determine the size of NPs as well as the polydispersity index (PDI) employing a DynaPro MS/X, (Wyatt Inc., Santa Barbara, CA, USA). Dry NPs were re-suspended in deionized water and sonicated for 10 min to improve dispersion homogeneity. Every sample was housed in quartz cuvettes and measured 40 times in one run.

2.1.4.3. Encapsulation efficiency (EE) and drug-loading capacity (LC) estimations. The encapsulation efficiency and loading capacity of MTL-loaded NPs were determined by a direct method with HPLC analysis. The samples were analyzed in an Agilent Zorbax SB C18: 3.5 μm x 50 mm×4.6 mm and dynamic multiple reaction monitoring spectra were acquired using a HPLC-QQQ Agilent 1260LC system. The entrapped drug was detected by direct injection of the samples after breaking the nanoparticles as follows: 1.0 mg of NPs were dissolved in 5 mL of acetonitrile:DMSO (1:1) mixture and sonicated for 25 min. Then, the solution was filtered over a 0.22 μm filter (Minisart® Syringe Filter, Polietersulfone (PES), ethylene oxide) and analyzed. The encapsulation efficiency and drug-loading capacity values were expressed according to the following Equations:

EE % = (MTL entrapped / MTL total) x 100

LC % = (MTL entrapped / NPs total) x 100

For the calibration curve, five standard solutions at concentrations ranging from 0.1 to 0.5 mg/mL of the three MTLs were prepared and analyzed under the same conditions.

2.2. Pharmacological evaluation

2.2.1. Prediction of the permeability through the blood-brain barrier using parallel artificial membrane permeability assay

Seven commercial drugs of known BBB permeability, namely atenolol, caffeine, enoxacine, piroxicam, testosterone, promazine and verapamile, were used as controls in each experiment to validate the analysis set. Controls and nanoparticle formulations were dissolved in 5 mL of the experimental buffer (phosphate buffer saline solution at pH 7.4 PBS/DMSO (95:5 respectively)). The donor 96-well plate (Millipore, catalog no. MAIPS4510) was filled with 180 μL of each compound solution after being coated with 4 μL of porcine brain lipid in dodecane (20 mg/mL) (Avanti Polar Lipids, catalog no. 141101). The acceptor 96-well plate (Millipore, catalog no. 141101) was filled with 180 μL of the experimental buffer. Then, the donor plate was carefully put on the acceptor plate to form a "sandwich" for 4 h and 30 min at room temperature. During the incubation time, compounds diffused from the donor plate through the brain−lipid membrane into the acceptor plate. After incubation, the donor plate was removed, and the concentration of the compounds was determined in the acceptor and the donor plates by MS spectrometry using an HPLC-QQQ Agilent 1260LC equipment. Every sample was analyzed using molecular weight detection in three wells and in two independent runs. Results are given as the mean ± standard deviation (SD) of the two runs. Commercial drugs, PBS, ethanol, and dodecane were purchased from Sigma, Acros organics, Merck, Aldrich, and Fluka.

2.2.2. Evaluation of in vitro inhibitory activity

2.2.2.1. Casein kinase 1. Compounds were screened using Kinase-Glo kit (Promega Biotech Ibérica S.L.). 10 μl of test compound (from 1 mM DMSO stock solution) were dissolved to the desired concentration in

assay buffer and mixed with 10 μl (16 ng) of enzyme followed by 20 μl of assay buffer containing 0.1 % casein as substrate and 4 μM of adenosine triphosphate (ATP). The final DMSO concentration in the reaction mixture did not exceed 1 %. After 60 min incubation at 30 °C the enzymatic reaction was stopped with 40 μl of Kinase-Glo reagent. Glow-type luminescence was recorded after 10 min using a FLUOstar Optima (BMG Labtechnologies GmbH, Offenburg, Germany) multimode reader. The activity is proportional to the difference of the total and consumed ATP. The inhibitory activities were calculated on the basis of maximal activities measured in the absence of inhibitor.

2.2.2.2. Leucine-rich repeated kinase 2. LRRK2 inhibitors were screened by ThermoFisher Scientific following the Adapta™ screening protocol. First, 200 μM ERM (LRRKtide) in 25 mM Tris / 7.5 mM HEPES pH 8.2, 0.005 % Brij-35,5 mM $MgCl_2$, 0.5 mM EGTA, 0.01 % NaN_3, ATP and 3.75–70 ng LRRK2 are added to the well, and the reaction is allowed to incubate for 60 minutes. Then, 5 μL of Detection Mix consisting of a europium labeled anti-ADP antibody, an Alexa Fluor™ 647 labeled ADP tracer, and EDTA (to stop the kinase reaction) is added to the assay well. ADP formed by the kinase reaction (in the absence of an inhibitor) will displace the Alexa Fluor 647 labeled ADP tracer from the antibody, resulting in a decrease in the TR-FRET signal. In the presence of an inhibitor, the amount of ADP formed by the kinase reaction is reduced, and the resulting intact antibodytracer interaction results in a high TR-FRET signal. ADP formation is determined by calculating the emission ratio from the assay well.

2.2.2.3. Tau tubulin kinase 1. The compounds are added to an empty plate at the desired concentration, then the following mixture is added: TTBK1 (human recombinant enzyme) (5−20 mU diluted in 50 mM Tris pH 7.5, 0.1 mM EGTA, 0.1 % β-mercaptoethanol, 1 mg/mL BSA, and 10 mM DTT) was assayed against RRKDLHDDEEDEAMSITA in a final volume of 25.5 μL, which contained 50 mM Tris pH 7.5, 0.1 mM EGTA, 0.3 mM RRKDLHDDEEDEAMSITA, 10 mM magnesium acetate, and 0.005 mM [33 P-γ-ATP] (50−1000 cpm/pmol). The reaction was incubated for 30 min at room temperature. Assays were stopped by addition of 5 μL of 0.5 M (3 %) orthophosphoric acid and then harvested onto P81 Unifilter plates with a wash buffer of 50 mM orthophosphoric acid.

2.2.2.4. Beta-secretase 1. BACE1 in vitro assays were carried out using FRET. An APP-based peptide substrate (rhodamine-EVNLDAEFK-quencher, *K*m of 20 μM) carrying the Swedish mutation and containing a rhodamine as a fluorescence donor and a quencher acceptor at each end was used. The intact substrate is weakly fluorescent and becomes highly fluorescent upon enzymatic cleavage. The assays were conducted in 50 mM sodium acetate buffer pH 4.5, in a final enzyme concentration (1 U/mL). Inhibitor screening at 10 μM. The mixture was incubated for 60 min at 25 °C under dark conditions and then stopped by addition of 2.5 M sodium acetate. Fluorescence was measured with a FLUOstar Optima (BMG Labtechnologies GmbH, Offenburg, Germany) microplate reader at 545 nm excitation and 585 nm emission.

2.2.3. Cell culture and treatments

SK-N-MC cells expressing the human isoform APP695 (SK-APP cell line D1; SKAPP-D1) were established through the transfection of SK-N-MC cells with a pCDNA3-APP expression vector, generously provided by Dr. MJ Bullido. These cells were cultured in DMEM (Thermo Fisher) medium supplemented with 10 % FBS (Thermo Fisher), 1 mM glutamine (Sigma-Aldrich), and 100 units/mL penicillin (Lonza), as well as 100 mg/mL streptomycin (Lonza). The cell cultures were maintained in a 5 % CO_2, humidified atmosphere at 37 °C.

Human neuroblastoma SH-SY5Y cell line was cultured in Dulbecco's Modified Eagle Medium (DMEM, VWR) supplemented with 10 % fetal bovine serum (FBS, Gibco) and 1 % penicillin-streptomycin (VWR) at 37 ºC and 5 % CO_2. One hundred thousand cells were seeded onto 96-well plates and treated with NPs and MTL at 1 μM. Twenty-four hours after 3-(4,5-dimethythiazol-2-yl)-2,5-diphenyl tetrazolium bromide (MTT) assay was performed. For neuroprotection assays, one hundred thousand cells were treated with NPs and MTLs at 0.5 μM (drug final concentration) and 1 h later with okadaic acid (OA) or ethacrynic acid (EA). Twenty-four hours later, MTT assay was carried out, thiazolyl blue was added to the culture media at final concentration of 0.25 mg/mL for at least 2 h at 37 ºC. After the incubation, culture media was removed and formazan crystals were dissolved with DMSO. Absorbance at 595 nm was measured with a plate reader (Synergy H4 Hibrid Reader, Biteck Instruments).

2.2.3.1. Measurements of cell viability. Cell viability was assessed using a 3-(4,5-dimethyl-2-thiazolyl)-2,5-diphenyl-2 H-tetrazolium bromide (MTT) assay (Sigma-Aldrich) in 96-well cell culture plates. After incubating all cells with a 0.5 mg/mL MTT solution (Sigma-Aldrich) at 37 °C for 4 h, followed by treatment with cell lysis buffer (20 % SDS, 50 % N, N-dimethylformamide, pH 4.7) for 3 h, absorbance values were determined at 590 nm. Cell viability was expressed as a percentage of the optical density (OD) of control cells, where the value was defined as 100 %.

For SH-SY5Y cells, the same procedure was followed, but cells were seeded in 24-well multiplates. Absorbance was measured using a Varioskan Flash multiplate reader (Thermo Scientific) at test wavelengths of 550 nm and reference wavelengths of 664 nm. The compound concentration for the SK-APP line was 10 μM, while for the SH-SY5Y line, concentrations of 1 and 5 μM were used. Okadaic acid (OA, Sigma-Aldrich) was initially dissolved in DMSO to create an initial stock concentration of 60 μM, from which a 250X working solution was derived through dilution in DMEM.

The compounds, prepared as 250X solutions, were directly introduced into the wells at the specified final concentrations, and this was done 1 h before treating with OA at a final concentration of 30 nM. DMSO was added at the appropriate concentration to the control-untreated cells. The cells were then maintained in the presence of OA and the various compounds for a period of 24 h.

2.2.3.2. Immunoassays. Levels of $A\beta_{40}$ and $A\beta_{42}$ were quantified from cellular lysates and conditioned media using sandwich enzyme-linked immunosorbent assays (ELISAs) (Wako, Osaka, Japan).

3. Results and discussion

3.1. Synthesis and biological activity of new multitarget compounds

Given the potential demonstrated by our previous MTLs [19], we have designed new compounds with inhibitory activity against tau and tubulin kinase 1 (TTBK1), using click chemistry for the synthesis of MTLs. This target has been explored recently and its inhibitors have shown to reduce TDP-43 phosphorylation *in vivo*, promote a shift to anti-inflammatory microglia and protect motor neurons in an ALS mouse model [22]. For the design of the new alkyne, we examined previous crystallographic and molecular dynamics studies performed in house on our validated TTBK1 inhibitors, leading to the introduction of the alkyne group at the para position of the phenyl ring in derivative **2**. This modification would enable the compound to react with an azide in a classical copper-catalyzed azide-alkyne cycloaddition. Previously reported compounds with CK1 and LRRK2 inhibitory properties (depicted as **6** and **7** in Fig. 2) were used as such azides. As a result, compounds **8** and **9** may serve as modulators of three pathological cascades (tau, TDP-43 and beta-amyloid) present in different NDs.

For this purpose, we synthesized alkyne **5**, that was later reacted with azides **6** and **7** to yield triazoles **8** and **9** (Scheme 1). The reaction conditions employed were specific to click-chemistry, previously optimized for this type of heterocycles in our laboratory [18]. All the newly

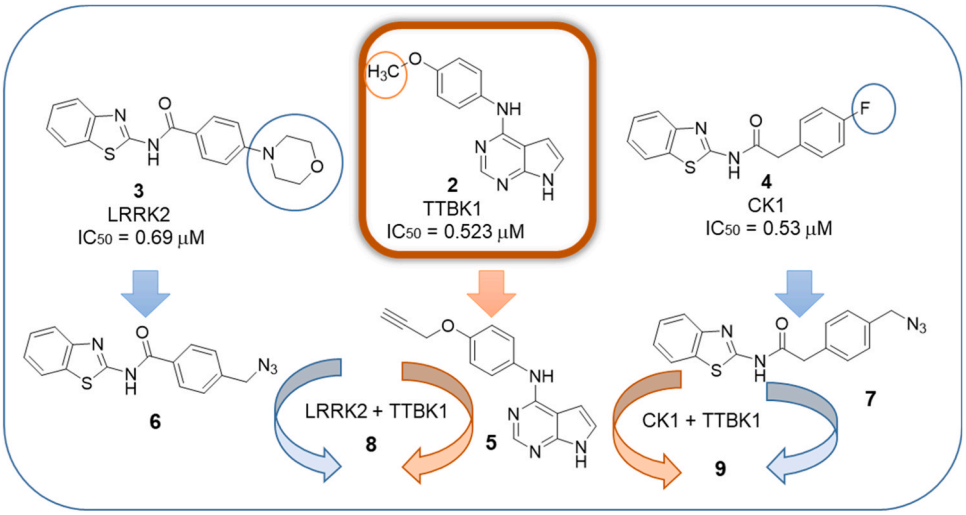

Fig. 2. Design of MTLs from different kinase inhibitors.

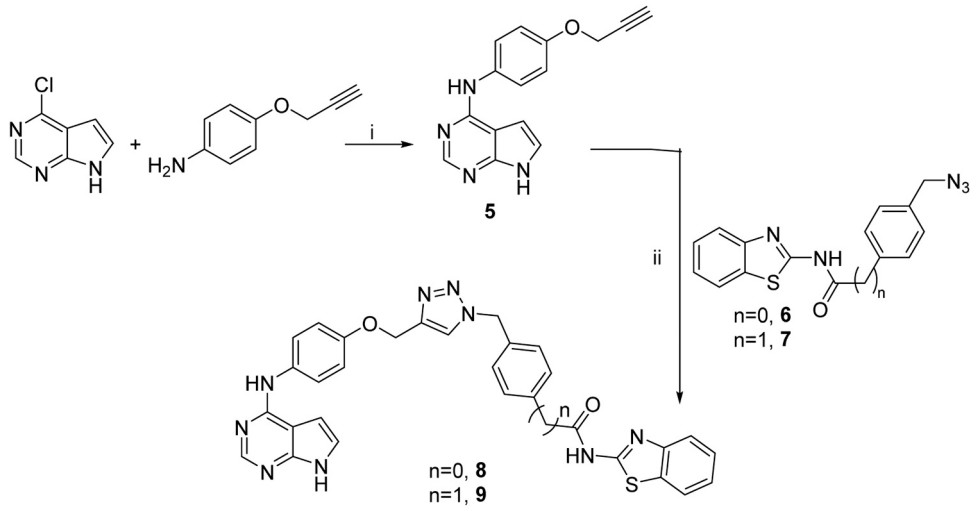

Scheme 1. Synthesis of the multitarget compounds 8 and 9. (i) $InCl_3$ (0.1 equiv), MW, MeCN, 100 °C; (ii) $CuSO_4$ (0.1 equiv), tris(benzyltriazolylmethyl)amine (0.1 equiv), sodium ascorbate (0.2 equiv), DMF, r.t.

synthetized compounds were isolated, purified and fully characterized using analytical and spectroscopic methods (^1H and ^{13}C NMR) (see Materials and Methods).

After the *in vitro* biological evaluation of the compounds **8** and **9** in human recombinant kinases using KinaseGlo methodology, both molecules were found to inhibit their corresponding target kinases with similar potency or with a slight decrease in IC_{50} (Table 1) compared to their previous precursors (Fig. 2). As we had previously shown that these type of molecular scaffolds may interact with BACE1 [19], we also evaluated this activity for both MTLs. Compound **8** exhibited low micromolar inhibition of BACE1 whereas compound **9** was a slightly less potent BACE1 inhibitor.

Table 1
Enzymatic activity of the new synthesized compounds together with the reported activity of their alkyne precursor.

Compound	CK1 IC_{50} (μM)	TTBK1 IC_{50} (μM)	LRRK2 IC_{50} (μM)	BACE1 IC_{50} (μM)
5	-	2.44 ± 0.08	-	-
8	-	4.20 ± 1.13	0.24 ± 0.06	0.68 ± 0.10
9	17.52 ± 1.20	0.11 ± 0.01	-	6.81 ± 0.19

Next, we decided to evaluate the potential of these newly synthesized MTLs in representative cellular models of NDs. We used okadaic acid (OA) and the human neuroblastoma cell line SH-SY5Y to emulate AD pathology where the cell death is produced by the increase of tau phosphorylation [23]. MTLs **8** and **9**, containing fragments trageting tau phosphorylation kinases in their chemical structure, were tested at two different concentrations (1 and 5 μM), along with the combination of the individual kinase inhibitors that comprise the MTLs. It was demonstrated that MTLs exhibited improved neuroprotective properties than the combination of the two kinase inhibitors, confirming our initial hypothesis of cooperative biological potential (Fig. 3).

MTL **9** contains two different fragments with kinase activity targeting TDP-43, CK1 and TTBK1. Therefore, it was assayed in a cellular model that emulates TDP-43 pathology present in ALS or FTD. SH-SY5Y cells were treated with ethacrynic acid, leading to an increase in TDP-43 phosphorylation and induction of cell death [24]. The individual kinase inhibitors, compounds **2** and **4**, their combination, and MTL **9** were tested at 0.5 μM showing that both the drug combination and the MTL treatment exert a significant neuroprotective effect (Fig. 4).

Finally, considering the strong ability of MTL **8** to modulate BACE1, this compound was tested in the SK-APP cellular line. This human neuroblastoma line is transfected with the precursor amyloid protein,

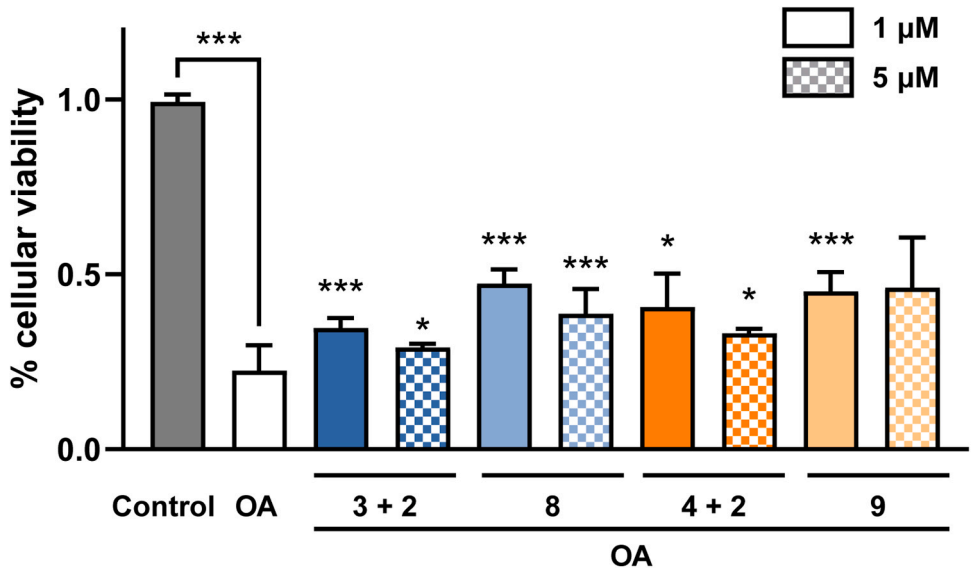

Fig. 3. Effects of MTLs **8** and **9** and their protein kinase inhibitors precursors on the viability of SH-SY5Y cells treated with OA (in white). Cells were treated at the indicated doses with the combination of the individual kinase inhibitors or the multitarget triazoles. Results expressed as % of control (DMSO) as the mean (± SEM) of at least three independent experiments performed in triplicate. (*p<0.05, **p<0.005, ***p<0.001 vs treatment with OA only).

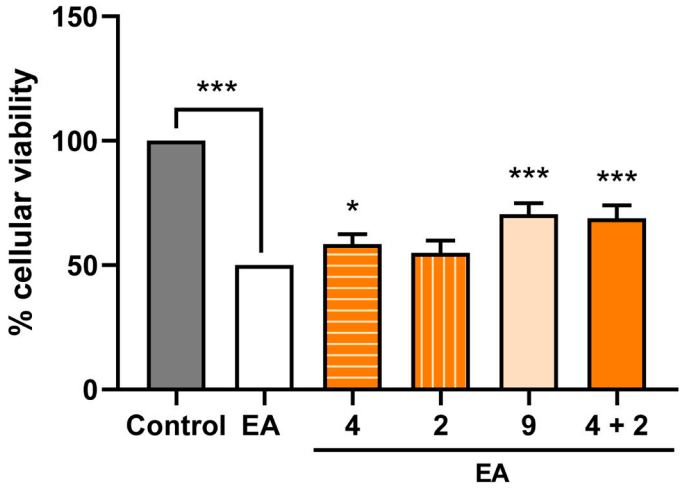

Fig. 4. Effect of MTL **9** and its protein kinase inhibitor precursors on the viability of SH-SY5Y cells treated with EA (50 μM) (in white). Cells were treated with protein kinase inhibitors, the combination of the individual kinase inhibitors or the multitarget triazole at 0.5 μM. Results expressed as % of control (DMSO) as the mean (± SEM) of at least three independent experiments performed in triplicate. (*p<0.05, ***p<0.001 vs treatment with EA only).

producing greater levels of beta-amyloid (Aβ). After checking the viability of the cells (Figure S1), we tested the potential of the BACE1 inhibitor MTL **8** to decrease the levels of $A\beta_{40}$ and $A\beta_{42}$ at a dose of 10 μM. Levels of $A\beta_{40}$ and $A\beta_{42}$ were measured in both cellular lysates and extracellular media, showing a significant reduction of $A\beta_{40}$ in both the biological matrix and significantly lower $A\beta_{42}$ levels in the extracellular media (Fig. 5).

After confirming the therapeutic potential of these compounds for the treatment of NDs such as AD or ALS, we decided to investigate their permeability across the blood brain barrier (BBB) using the parallel artificial membrane permeability assay (PAMPA) methodology, as these compounds need to reach the central nervous system to exert its efficacy. However, the insolubility of compound **8** in the assay conditions impeded the calculation of its permeability value (P_e) whereas for triazole **9,** the experimental permeability value P_e was of $0.2 \pm 0.01 \times 10^{-6}$ cm s^{-1} which is not compatible with BBB permeation and thus classified as negative (CNS-).

The data obtained in the permeability assay confirmed the difficulty of large multitarget compounds in penetrating the BBB through passive diffusion while maintaining favorable pharmacokinetic characteristics. This difficulty had also been observed for the previously reported MTL **1**. At this point, we opted to encapsulate these three MTLs using organic polymeric nanoparticles composed of polylactic-co-glycolic acid (PLGA) to address the poor permeability of the compounds.

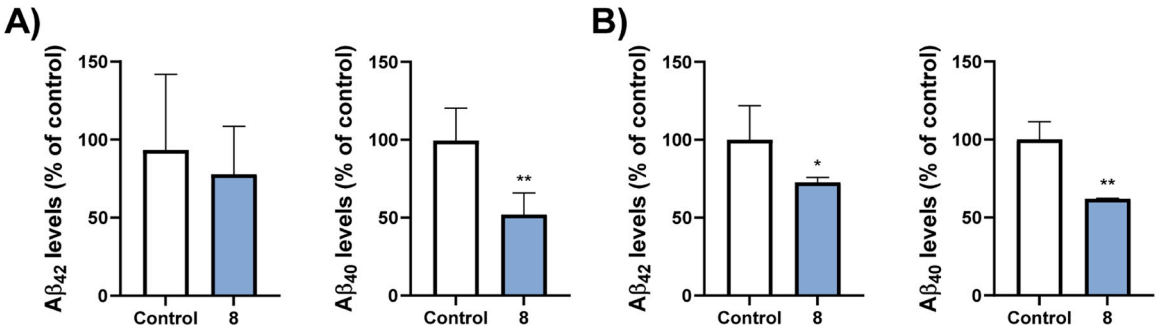

Fig. 5. Reduced levels of $A\beta_{42}$ and $A\beta_{40}$ in SK-APP cells after 48 h treatment with compound **8** at 10 μM. A) cellular lysates; B) extracellular media. Data are presented as mean ± SEM of at least three independent experiments performed in triplicate (*p<0.05; **p<0.01).

3.2. Preparation and optimization of PLGA nanoparticles

Nanoparticles made of PLGA have demonstrated successful BBB permeation in previous studies [25–27]. Furthermore, PLGA is one of the few polymers approved by the Food and Drug Administration (FDA) for clinical use based on its extensive safety properties. PLGA nanoparticles exhibit biocompatibility with cells and tissues, as they undergo hydrolysis to produce lactic and glycolic acids, which are naturally metabolized in the body [28].

For the preparation of the organic nanoparticles, the nanoprecipitation methodology was selected. This is a one-step method where the polymer and the drug are dissolved in a water-miscible organic solution, which is then added to an aqueous phase containing a surfactant, in our case, polyvinyl alcohol (PVA). The rapid diffusion of the organic solvent in the aqueous phase drives the formation of NPs, which are stabilized by the surfactant. Optimization of the synthetic procedure was performed with the new MTLs **8** and **9,** varying the proportion of organic solvent mixture (acetone, DMSO) and the initial quantity of compound (5 and 10 mg). In all the different conditions tested, each performed at least in duplicate, 50 mg of PLGA and 500 mg of PVA were used.

Results obtained are described in Table 2. From these studies we concluded that the best nanoparticle formation methodology was achieved by encapsulating 10 mg of MTL using a 1:1 acetone:DMSO proportion as solvent. Following these parameters, NPs of MTL **1** were as well prepared (Table 2).

3.3. Characterization of PLGA nanoparticles

The prepared PLGA nanoparticles loaded with the different MTLs were physically and biologically characterized.

3.3.1. Morphology and size of nanoparticles

As the replicates of the formulations were similar, we selected one formulation obtained under optimized conditions for each MTLs (NP1.1, NP8.9 and NP9.7) for further characterization. The morphology of the nanoparticles was assessed using scanning electron microscopy (SEM). Upon direct visualization of the sample, which was previously coated with a thin layer of gold to enhance conductivity, the nanoparticles exhibited a spherical and smooth shape, as illustrated in various SEM images in Fig. 3A, S2 and S3, with an approximate size of 100 nm.

For a more precise determination of the size of MTL-loaded NPs, dynamic light scattering (DLS) technique was employed [29]. DLS results (Fig. 6B, S3 and S4) indicated a hydrodynamic radius (R_h) between 117 and 143 nm for the three formulations, a size compatible with effective drug delivery to the brain [27]. Furthermore, the polydispersity index (PDI), employed to assess the average uniformity of a particle solution, was calculated. The PDI values obtained (<0.2) signify a monodisperse particle suspension with a narrow size distribution. Another observation that emerged from this data was the slight variability in terms of size in the nanoparticles due to the use of DMSO in the nanoprecipitation, which was accompanied by a more agglomerated aspect of the formulations.

Table 2
Formulations for MTLs **8, 9** and **1** drug-loaded nanoparticles preparation using 50 mg of PLGA and 500 mg of PVA.

MTL	Formulation	Compound quantity (mg)	Solvent proportion Acetone:DMSO	NPs quantity (mg)
8	NP8.1	5.0	4:1	15.2
	NP8.2	5.0	4:1	15.5
	NP8.3	5.0	1:1	17.2
	NP8.4	5.0	1:1	18.0
	NP8.5	10.0	4:1	17.0
	NP8.6	10.0	4:1	18.3
	NP8.7	10.0	4:1	17.7
	NP8.8	10.0	4:1	14.6
	NP8.9	10.0	1:1	13.7
	NP8.10	10.0	1:1	20.4
9	NP9.1	5.0	4:1	16.0
	NP9.2	5.0	4:1	16.9
	NP9.3	5.0	1:1	17.8
	NP9.4	5.0	1:1	26.0
	NP9.5	10.0	4:1	14.0
	NP9.6	10.0	4:1	14.2
	NP9.7	10.0	1:1	23.7
	NP9.8	10.0	1:1	26.6
	NP1.1	10.0	1:1	18.7
1	NP1.2	10.0	1:1	19.2
	NP1.3	10.0	1:1	23.3
	NP1.4	10.0	1:1	22.4

3.3.2. Encapsulation efficiency and drug-loading capacity

Next, we calculated the encapsulation efficiency (EE) as well as the loading capacity (LC) for formulations prepared under the optimized conditions. Both parameters were determined using a direct method employing high-performance liquid chromatography (HPLC) analysis of the entrapped MTL after breaking the NPs with an acetonitrile:DMSO solution followed by sonication, and were expressed according to the equations outlined in the experimental section. Previously, calibration curves for the three MTLs were prepared and analyzed under the same conditions. The results, presented in Table 3 and S1, indicate EE values around 50 % with an average LC of 27 %. These data are within the range of reported NPs and underscore the efficiency of encapsulating MTLs in PLGA nanoparticles trough the nanoprecipitation methodology [30].

3.3.3. BBB permeability of nanoparticle formulations

Next, we chose to assess the permeability of the selected formulations, aiming to confirm the enhanced BBB penetrance compared to the parent compounds. The evaluation was conducted using the PAMPA methodology, following the same procedure reported previously for the MTLs. The obtained permeability values are summarized in Table 4. For all three formulations, the anticipated permeability laid within the uncertainty range of BBB penetration, although these values represent a slight improvement over the parent compounds. Notably, the permeability of MTL **9** was increased by 11.5 times with the NP9.7 formulation, representing the highest enhancement observed.

3.3.4. Cell-based efficacy studies of nanoparticle formulations

As MTL-loaded PLGA NPs have shown a modestly increased permeability trough the BBB, we wanted to investigate the related improvement in NDs cellular models. Consequently, we performed evaluations of the neuroprotective properties of the PLGA formulations using the previously described cell-based models. Initially, viability studies were undertaken to confirm their safety at 1 μM (Figure S4). Subsequently, neuroprotection studies were performed at the lowest effective dose, determined to be 0.5 μM. The **NP9.7** formulation of MTL **9** was tested in both disease models (AD and ALS), while MTL **1** and **8** formulations (**NP1.4**, **NP8.9** respectively) were assessed only in the AD disease model (Fig. 7). These findings demonstrate that the NPs exhibited a neuroprotective effect that was either improved or comparable to the activity of the MTLs alone. In all cases, the NPs formulations enhanced the drug profile of the MTLs as the administered dose is one order of magnitude lower than that of the MTL alone.

4. Conclusions

In this study, we designed and synthesized two novel MTL (compounds **8** and **9**) exhibiting inhibitory activity against TTBK1, along with CK1 or LRRK2 and BACE1 inhibition. These compounds demonstrated enhanced pharmacological efficacy compared to individual fragments in cellular models of AD and ALS. Due to the suboptimal blood-brain barrier permeability of these compounds, PLGA nanoparticles were

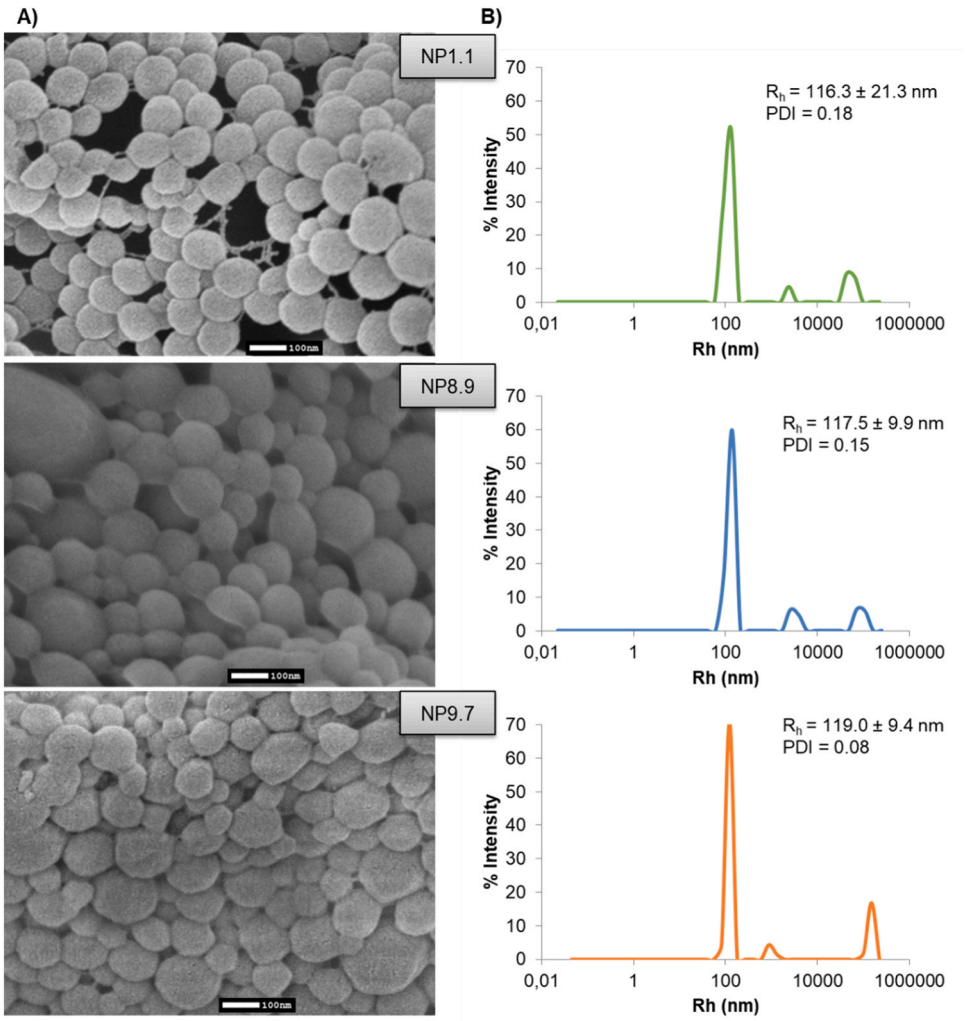

Fig. 6. A) SEM images of nanoparticles loaded with the different MTLs **1, 8** and **9**. B) Size distribution of MTL-loaded nanoparticles (NP1.4, NP8.9 and NP9.7). Results are shown as the mean of 40 measures ± standard deviation (SD) and were obtained by DLS. PDI refers to polydispersity of NPs.

Table 3
Percentages of encapsulation efficiency and loading capacity of the selected formulations.

MTL	Formulation	Amount of MTL encapsulated (mg)	EE %	LC %
1	NP1.1	5.18	52	60
	NP1.2	5.26	52	28
	NP1.3	3.64	37	16
	NP1.4	4.47	44	20
8	NP8.9	5.21	53	39
	NP8.10	3.70	37	18
9	NP9.7	4.05	41	17
	NP9.8	5.84	58	22

Table 4
Calculated permeability with the PAMPA methodology and expected CNS permeability prediction based on the model.

Formulation	P_e x10^{-6}cm s^{-1}	Permeability prediction
NP1.4	1.47	CNS +/-
NP8.9	1.75	CNS +/-
NP9.7	2.30	CNS +/-

synthesized under diverse methodological conditions and characterized using a range of physico-chemical and analytical techniques.

The BBB permeation of these NPs was evaluated using the PAMPA methodology, revealing that the encapsulation could moderately improve the expected permeability values of the compounds. Finally, upon comparing the therapeutic impact of these nanoparticles, it was demonstrated that the formulations provided better neuroprotection in cellular models of AD and ALS compared to the free MTL. Our results suggest that PLGA encapsulation could serve as a valid strategy to enhance permeability, increasing compound bioavailability within the cell and thereby enhancing their efficacy in cellular models. However, several parameters need to be taken into account when formulating new nanoparticles as these small changes greatly influence the outcome. Further *in vivo* studies will be required to assess CNS permeability of the nanoformulations to ultimately benchmark the use of multitarget ligands and their encapsulation in PLGA nanoparticles.

Funding

This work was supported by AIE (grant PID2019–105600RB-I00), La Caixa and Luzón foundations (grant HR21–00937) and MCIN/AEI /10.13039/501100011033 (grant RYC2019–027489-I).

CRediT authorship contribution statement

Loreto Martinez-Gonzalez: Writing – review & editing, Visualization, Validation, Investigation, Formal analysis, Data curation. **Eva Carro:** Writing – review & editing, Supervision, Formal analysis,

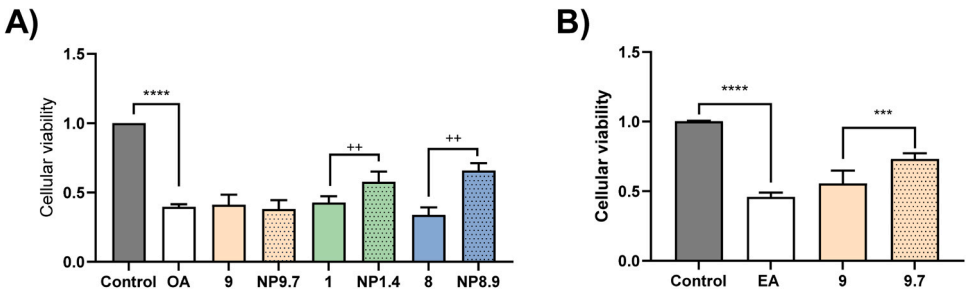

Fig. 7. Neuroprotection studies in SH-SY5Y cell line at 0.5 μM of each NP formulation and 0.5 μM of the corresponding MTL, EA and OA at 40 μM and 40 nm respectively. a) Neuroprotection in AD model. b) Neuroprotection in ALS model. Data are presented as the mean ± SEM of three independent experiments. (**** $p<0.0001$, *** $p<0.001$, ** $p<0.01$ by one-way ANOVA analysis; ++ $p<0.01$, + $p<0.1$ by t test analysis).

Conceptualization. **Alfonso Garcia-Rubia:** Writing – review & editing, Supervision, Investigation, Formal analysis, Data curation. **Vanesa Nozal:** Writing – review & editing, Writing – original draft, Visualization, Investigation, Data curation. **Paula Fernandez-Gomez:** Writing – review & editing, Investigation, Data curation. **Ana Martinez:** Writing – review & editing, Writing – original draft, Supervision, Funding acquisition, Formal analysis, Conceptualization. **Eva P Cuevas:** Writing – review & editing, Visualization, Validation, Investigation, Formal analysis, Data curation. **Valle Palomo:** Writing – review & editing, Writing – original draft, Supervision, Methodology, Formal analysis, Conceptualization.

Declaration of Competing Interest

The authors declare the following financial interests/personal relationships which may be considered as potential competing interests: Ana Martinez, Valle Palomo reports financial support was provided by AEI. Ana Martinez, Valle Palomo reports financial support was provided by La Caixa and Luzón Foundation. If there are other authors, they declare that they have no known competing financial interests or personal relationships that could have appeared to influence the work reported in this paper.

Data Availability

Data will be made available on request.

Acknowledgements

We are grateful to the Analysis Service Unit facilities of ICTAN-CSIC for the analysis of Chromatography and Mass Spectrometry and to the CAIs of Microscopy and Nuclear Magnetic Resonance from UCM for their support in SEM images and NMR spectra.

Appendix A. Supporting information

Supplementary data associated with this article can be found in the online version at doi:10.1016/j.biopha.2024.116626.

References

[1] K.S. Dias, C. Viegas, Multi-target directed drugs: a modern approach for design of new drugs for the treatment of Alzheimer's disease, Curr. Neuropharmacol. *12* (3) (2014) 239–255, https://doi.org/10.2174/1570159×1203140511153200.
[2] C.J. Van der Schyf, The use of multi-target drugs in the treatment of neurodegenerative diseases, Expert Rev. Clin. Pharmacol. 4 (3) (2011) 293–298, 210 1586/ecp 1511 1513.
[3] M.L. Bolognesi, Polypharmacology in a single drug: multitarget drugs, Curr. Med. Chem. *20* (13) (2013) 1639–1645, 16102174/0929867311320130004.
[4] D.S. Knopman, H. Amieva, R.C. Petersen, G. Chételat, D.M. Holtzman, B.T. Hyman, R.A. Nixon, D.T. Jones, Alzheimer disease, Nat. Rev. Dis. Prim. *7* (1) (2021) 33, https://doi.org/10.1038/s41572-021-00269-y.
[5] M. Neumann, D.M. Sampathu, L.K. Kwong, A.C. Truax, M.C. Micsenyi, T.T. Chou, J. Bruce, T. Schuck, M. Grossman, C.M. Clark, et al., Ubiquitinated TDP-43 in frontotemporal lobar degeneration and amyotrophic lateral sclerosis, Science *314* (5796) (2006) 130–133, https://doi.org/10.1126/science.1134108.
[6] A. Meneses, S. Koga, J. O'Leary, D.W. Dickson, G. Bu, N. Zhao, TDP-43 pathology in Alzheimer's disease, Mol. Neurodegener. *16* (1) (2021) 84, https://doi.org/10.1186/s13024-021-00503-x.
[7] P.T. Nelson, D.W. Dickson, J.Q. Trojanowski, C.R. Jack, P.A. Boyle, K. Arfanakis, R. Rademakers, I. Alafuzoff, J. Attems, C. Brayne, et al., Limbic-predominant age-related TDP-43 encephalopathy (LATE): consensus working group report, Brain *142* (6) (2019) 1503–1527, https://doi.org/10.1093/brain/awz099.
[8] V. Palomo, V. Nozal, E. Rojas-Prats, C. Gil, A. Martinez, Protein kinase inhibitors for amyotrophic lateral sclerosis therapy, Br. J. Pharmacol. *178* (6) (2021) 1316–1335, https://doi.org/10.1111/bph.15221.
[9] C.L. Benn, L.A. Dawson, Clinically precedented protein kinases: rationale for their use in neurodegenerative disease, Front. Aging Neurosci. *12* (2020) 242, https://doi.org/10.3389/fnagi.2020.00242 (From NLM PubMed-not-MEDLINE).
[10] A. Lui, J. Vanleuven, D. Perekopskiy, D. Liu, D. Xu, O. Alzayat, T. Elgokhy, T. Do, M. Gann, R. Martin, D.Z. Liu, FDA-approved kinase inhibitors in preclinical and clinical trials for neurological disorders, Pharmaceuticals *15* (12) (2022), https://doi.org/10.3390/ph15121546.
[11] L. Sereno, M. Coma, M. Rodriguez, P. Sanchez-Ferrer, M.B. Sanchez, I. Gich, J. M. Agullo, M. Perez, J. Avila, C. Guardia-Laguarta, et al., A novel GSK-3beta inhibitor reduces Alzheimer's pathology and rescues neuronal loss in vivo. Neurobiol. Dis. *35* (3) (2009) 359–367, https://doi.org/10.1016/j.nbd.2009.05.025.
[12] D. Koehler, Z.A. Shah, F.E. Williams, The GSK3beta inhibitor, TDZD-8, rescues cognition in a zebrafish model of okadaic acid-induced Alzheimer's disease. Neurochem. Int. *122* (2019) 31–37, https://doi.org/10.1016/j.neuint.2018.10.022.
[13] S. Lovestone, M. Boada, B. Dubois, M. Hull, J.O. Rinne, H.J. Huppertz, M. Calero, M.V. Andres, B. Gomez-Carrillo, T. Leon, et al., A phase II trial of tideglusib in Alzheimer's disease, J. Alzheimer's Dis. *45* (1) (2015) 75–88, https://doi.org/10.3233/JAD-141959.
[14] L. Martinez-Gonzalez, E.P. Cuevas, C. Tosat-Bitrián, V. Nozal, C. Gil, V. Palomo, Á. Martín-Requero, A. Martinez, TTBK1 and CK1 inhibitors restore TDP-43 pathology and avoid disease propagation in lymphoblast from Alzheimer's disease patients, Front. Mol. Neurosci. *16* (2023) 1243277, https://doi.org/10.3389/fnmol.2023.1243277.
[15] L. Martinez-Gonzalez, C. Rodriguez-Cueto, D. Cabezudo, F. Bartolome, P. Andres-Benito, I. Ferrer, C. Gil, A. Martin-Requero, J. Fernandez-Ruiz, A. Martinez, E. de Lago, Motor neuron preservation and decrease of in vivo TDP-43 phosphorylation by protein CK-1delta kinase inhibitor treatment. Sci. Rep. *10* (1) (2020) 4449, https://doi.org/10.1038/s41598-020-61265-y.
[16] D. Jennings, S. Huntwork-Rodriguez, M. Vissers, V.M. Daryani, D. Diaz, M.S. Goo, J.J. Chen, R. Maciuca, K. Fraser, O.S. Mabrouk, et al., LRRK2 inhibition by BIIB122 in healthy participants and patients with Parkinson's disease, Mov. Disord. *38* (3) (2023) 386–398, https://doi.org/10.1002/mds.29297.
[17] S. Castro-Sanchez, J. Zaldivar-Diez, E. Luengo, M.G. Lopez, C. Gil, A. Martinez, I. Lastres-Becker, Cognitive enhancement, TAU phosphorylation reduction, and neuronal protection by the treatment of an LRRK2 inhibitor in a tauopathy mouse model, Neurobiol. Aging *96* (2020) 148–154, https://doi.org/10.1016/j.neurobiolaging.2020.09.006.
[18] R. Benítez-Fernández, F. Josa-Prado, E. Sánchez, Y. Lao, A. García-Rubia, J. Cumella, A. Martínez, V. Palomo, F. de Castro, Efficacy of a benzothiazole-based LRRK2 inhibitor in oligodendrocyte precursor cells and in a murine model of multiple sclerosis, CNS Neurosci. Ther. *30* (2024) e14552.
[19] V. Nozal, A. Garcia-Rubia, E.P. Cuevas, C. Perez, C. Tosat-Bitrian, F. Bartolome, E. Carro, D. Ramirez, V. Palomo, A. Martinez, From Kinase inhibitors to multitarget ligands as powerful drug leads for Alzheimer's disease using protein-templated synthesis, Angew. Chem. Int. Ed. Engl. *60* (35) (2021) 19344–19354, https://doi.org/10.1002/anie.202106295.
[20] N.F. Liachko, P.J. McMillan, T.J. Strovas, E. Loomis, L. Greenup, J.R. Murrell, B. Ghetti, M.A. Raskind, T.J. Montine, T.D. Bird, et al., The tau tubulin kinases TTBK1/2 promote accumulation of pathological TDP-43, PLoS Genet. *10* (12) (2014) e1004803, https://doi.org/10.1371/journal.pgen.1004803.
[21] M.C. Operti, A. Bernhardt, S. Grimm, A. Engel, C.G. Figdor, O. Tagit, PLGA-based nanomedicines manufacturing: technologies overview and challenges in industrial

scale-up, Int. J. Pharm. *605* (2021) 120807, https://doi.org/10.1016/j.ijpharm.2021.120807.
[22] V. Nozal, L. Martínez-González, M. Gomez-Almeria, C. Gonzalo-Consuegra, P. Santana, A. Chaikuad, E. Pérez-Cuevas, S. Knapp, D. Lietha, D. Ramírez, et al., TDP-43 modulation by Tau-Tubulin Kinase 1 inhibitors: a new avenue for future amyotrophic lateral sclerosis therapy, J. Med. Chem. *65* (2) (2022) 1585–1607, https://doi.org/10.1021/acs.jmedchem.1c01942.
[23] M. Boban, M. Babic Leko, T. Miskic, P.R. Hof, G. Simic, Human neuroblastoma SH-SY5Y cells treated with okadaic acid express phosphorylated high molecular weight tau-immunoreactive protein species, J. Neurosci. Methods *319* (2019) 60–68, https://doi.org/10.1016/j.jneumeth.2018.09.030.
[24] Y. Iguchi, M. Katsuno, S. Takagi, S. Ishigaki, J. Niwa, M. Hasegawa, F. Tanaka, G. Sobue, Oxidative stress induced by glutathione depletion reproduces pathological modifications of TDP-43 linked to TDP-43 proteinopathies, Neurobiol. Dis. *45* (3) (2012) 862–870, https://doi.org/10.1016/j.nbd.2011.12.002.
[25] E. Rojas-Prats, C. Tosat-Bitrian, L. Martinez-Gonzalez, V. Nozal, D.I. Perez, A. Martinez, Increasing brain permeability of PHA-767491, a cell division cycle 7 kinase inhibitor, with biodegradable polymeric nanoparticles, Pharmaceutics *13* (2) (2021), https://doi.org/10.3390/pharmaceutics13020180.
[26] V. Nozal, E. Rojas-Prats, I. Maestro, C. Gil, D.I. Perez, A. Martinez, Improved controlled release and brain penetration of the small molecule S14 Using PLGA nanoparticles, Int. J. Mol. Sci. *22* (6) (2021), https://doi.org/10.3390/ijms22063206.
[27] J. Kreuter, Drug delivery to the central nervous system by polymeric nanoparticles: what do we know? Adv. Drug Deliv. Rev. *71* (2014) 2–14, https://doi.org/10.1016/j.addr.2013.08.008.
[28] H.K. Makadia, S.J. Siegel, Poly lactic-co-glycolic acid (PLGA) as biodegradable controlled drug delivery carrier, Polymers *3* (3) (2011) 1377–1397, https://doi.org/10.3390/polym3031377.
[29] P.M. Carvalho, M.R. Felicio, N.C. Santos, S. Goncalves, M.M. Domingues, Application of Light scattering techniques to nanoparticle characterization and development, Front. Chem. *6* (2018) 237, https://doi.org/10.3389/fchem.2018.00237.
[30] C. Wischke, S.P. Schwendeman, Principles of encapsulating hydrophobic drugs in PLA/PLGA microparticles, Int. J. Pharm. *364* (2) (2008) 298–327, https://doi.org/10.1016/j.ijpharm.2008.04.042.